RESEARCH ARTICLE

Macromolecular Materials and Engineering
Open Access
www.mame-journal.de

Negative Voltage Electrospinning for the Production of Highly Efficient PVDF Filters

*Carlo Gotti, Monica Torsello, Riccardo Onesti, Gianmarco Tanganelli, Alberto Sensini, Cristiana Boi, Davide Fabiani, Maria Letizia Focarete, and Andrea Zucchelli**

In recent years, the demand for filter media has increased dramatically, driven by the need to manufacture personal protective equipment and for various applications in the industrial and civil sectors. Nanofiber-based membranes are proposed as potential alternatives to commercial filtration devices. This study presents the design and implementation of an innovative pre-industrial electrospinning setup, combining a negatively charged spinneret and a positively charged counter-electrode, capable of producing polyvinylidene fluoride (PVDF) nanofibers with an average diameter of 410 nm and electrostatic surface potential values 3.7 times higher compared to a conventional electrospinning process, eliminating the need for further post-treatment. These properties are essential for improving mechanical and electrostatic filtration of small particles, including infectious droplets. The surface potential of the membranes is also long-lasting, as evidenced by tests one year after manufacture. As a case-study, these filters are used to manufacture surgical masks, reporting excellent performance in terms of bacterial filtration efficiency (BFE) up to 99.9%, and breathability (29.8±4.5 Pa cm^{-2}) when compared to commercially available meltblown polypropylene (PP) face masks, and also complied with the stringent European standard (EN14683:2019) for type-II surgical masks. Furthermore, the pre-industrial setup allows for increased production capacity of up to 42 000 m^2 per year, suitable for large-scale production.

1. Introduction

During the early stages of the Covid-19 pandemic, there was a global shortage of personal protective equipment, including face masks and respirators. The demand for these essential tools to prevent the transmission of Covid-19 exceeded the available supply. Although the World Health Organization declared the end of the COVID-19 global health emergency in May 2023, these years have demonstrated the importance of having multiple redundant strategies for the autonomous production of essential protective equipment in the event of an emergency. Currently, commercial air filters primarily consist of randomly arranged polymer fibers or glass fibers that passively trap particulate matter (PM) due to the porous structure of the fibrous membrane.[1] However, recent advances have focused on the development of innovative membrane filters that utilize electrostatic mechanisms to capture smaller PM, particularly in the 0.2–0.5 µm range, where mechanical filtration methods are less effective.[2]

C. Gotti, A. Zucchelli
Interdepartmental Centre for Industrial Research in Advanced Mechanical Engineering Applications and Materials Technology (CIRI-MAM)
Alma Mater Studiorum-University of Bologna
Bologna 40136, Italy
E-mail: a.zucchelli@unibo.it

M. Torsello, M. L. Focarete
Department of Chemistry "Giacomo Ciamician" and INSTM UdR of Bologna
Alma Mater Studiorum-University of Bologna
Bologna 40126, Italy

R. Onesti, C. Boi
Department of Civil
Chemical
Environmental and Materials Engineering (DICAM)
Alma Mater Studiorum–University of Bologna
Bologna 40131, Italy

G. Tanganelli, D. Fabiani
Department of Electrical
Electronic
and Information Engineering (DEI)
Alma Mater Studiorum-University of Bologna
Bologna 40136, Italy

A. Sensini, A. Zucchelli
Department of Industrial Engineering (DIN)
Alma Mater Studiorum-University of Bologna
Bologna 40136, Italy

A. Sensini
Department of Complex Tissue Regeneration and cell Biology-Inspired Tissue Regeneration
MERLN Institute for Technology-Inspired Regenerative Medicine
Maastricht University
Maastricht 6229ET, The Netherlands

The ORCID identification number(s) for the author(s) of this article can be found under https://doi.org/10.1002/mame.202300442

DOI: 10.1002/mame.202300442

Traditional electrostatic filters are challenged by manufacturing processes that result in irregular fiber and pore sizes.[3] In addition, the temporary electrostatic charge provided by corona discharge or triboelectric charging treatments[4,5] diminishes over time, limiting their effectiveness.[6,7] Disposable face masks and respirators, widely used during the pandemic, contribute to pollution[8] and offer limited comfort due to high air resistance.[9]

Nanofiber-based membranes, particularly those made of polyvinyl alcohol (PVA),[10,11] polyacrylonitrile (PAN),[12,13] polyurethane (PU),[14] polyamide (PA),[15,16] polysulfone (PSU),[17] and more recently PVDF,[9,18–23] have gained attention for their high filtration efficiency and breathability.[9,24–26] Electrospinning, the technique used to prepare these nonwoven micro- and nanofibrous materials, offers advantages such as high porosity and surface-to-volume ratio.[27,28]

Moreover, due to its versatility, electrospinning has been increasingly used in the development of advanced functional filtration masks.[29] This technique facilitates the incorporation of additional compounds into the polymer solution, enabling the infusion of antibacterial and antiviral properties into nanofibers, the implementation of self-sterilization mechanisms, and the incorporation of stimuli-responsive or energy-harvesting properties.[30] In addition, electrospinning is proving to be instrumental in enhancing conventional meltblown surgical masks through the addition of functionalized layers.[31] An important feature of electrospun membranes is that they can retain surface charges without additional treatments, providing electrostatic behavior similar to electret filters.[24] The small fiber diameter and pore size of nanofibrous membranes also enable mechanical filtration, unaffected by charge decay, making them superior to conventional microporous filters.[18]

PVDF, an easily electrospinnable semicrystalline polymer with various polymorphic structures, has excellent performance in piezoelectric and energy-harvesting devices.[4,32] During electrospinning, the stretching of the polymer solution promotes the α-to-β phase conversion.[9] β-PVDF, which has an all-trans conformation and an asymmetric distribution of fluorine atoms, generates electric dipoles. Polarization is maximized and stabilized with the polymer chains perpendicular to the dipole direction.[9] The charge storage ability of PVDF fibers facilitates the capture of fine particulate matter and aerosols, resulting in promising filtration efficiencies in terms of PM or Particle Filtration Efficiency (PFE) with aerosols loaded with different particle types and sizes.[18–21,33–36] However, few studies have evaluated the BFE of PVDF electrospun masks[37] according the European standard for surgical masks (EN14683:2019).[38]

The crystallization process and the conversion to the β-phase of the polymer are not the only factors that affect the electrical properties of PVDF electrospun fibers.[9] Several studies have focused their attention on investigating the effects of polarity on the formation of electrospun polymer fibers, and in particular, most studies on polymer electrospinning employ positive voltage, while a few have explored negative voltage to enhance surface charge.[39–42] The overall impact of negative voltage and its dependence on polymer and solvent properties remains unclear.[43] There is limited research on PVDF nanofibers obtained by negative voltage electrospinning for energy harvesting,[44] biological scaffolds,[45] and nanogenerators/strain sensors.[46] No previous studies have examined the influence of polarity on electrospun PVDF filters. Moreover, while several studies have developed electrospun filters for face masks,[1,47,48] there is limited information on their application in medical devices. This is primarily due to the fact that most studies have been conducted at the laboratory scale, producing small samples, whereas product validation based on regulatory standard requires large-scale production with consistent quality.

This work reports the development of electrospun PVDF nanofibrous membranes with enhanced filtration and breathability properties that meet the stringent European surgical mask standard. The employment of a customized pre-industrial electrospinning setup allowed the production of samples in large quantities for regulatory testing. The influence of the electrospinning polarity on the surface potential was investigated in order to maximize filtration through the electrostatic mechanism. In addition, surface potential measurements were performed one year after membrane production. The increased productivity achieved by the custom electrospinning system facilitated the transition from laboratory to industrial scale production, enabling testing in accordance with current regulations.

2. Experimental Section

2.1. Materials

PVDF powder (Kynar 741, Arkema Technical Polymers–Colombes (FR)) was kindly provided by GVS S.p.A. (Via Roma 50, 40 069, Zola Predosa, Bologna, Italy). N,N-Dimethylacetamide (DMAc), and Acetone (AC) were purchased from Sigma–Aldrich (Milan, Italy) and used without further purification. A spunbond PP roll of tissue (width = 17.5 cm) was kindly provided by KVM Engineering S.r.l.

2.2. Development of the Multi-needle Electrospinning Setup

To move from laboratory scale to pre-industrial production, a new electrospinning machine was designed ad hoc in collaboration with the Marchesini Group company (**Figure 1**). The machine was developed by converting and modifying a packaging machine. The machine is divided into two main chambers: the first (left side of Figure 1A) is dedicated to the handling, tensioning, and final collection of the spunbonded fabric; the second (right side of Figure 1A) houses the actual electrospinning process. The structure consists of an anodized aluminum frame, with both rooms enclosed by Plexiglas walls (Figure 1B), and a fume hood was added to the process room to eliminate solvent vapors.

The spunbond spool feeds a first mechanism, consisting of three cylinders, called the dancer roller, whose function is to regulate and maintain constant tension on the fabric. The spunbond

C. Boi, M. L. Focarete
Interdepartmental Centre for Industrial Research in Health Sciences and Technologies (CIRI-SDV)
Alma Mater Studiorum-University of Bologna
Bologna 40064, Italy

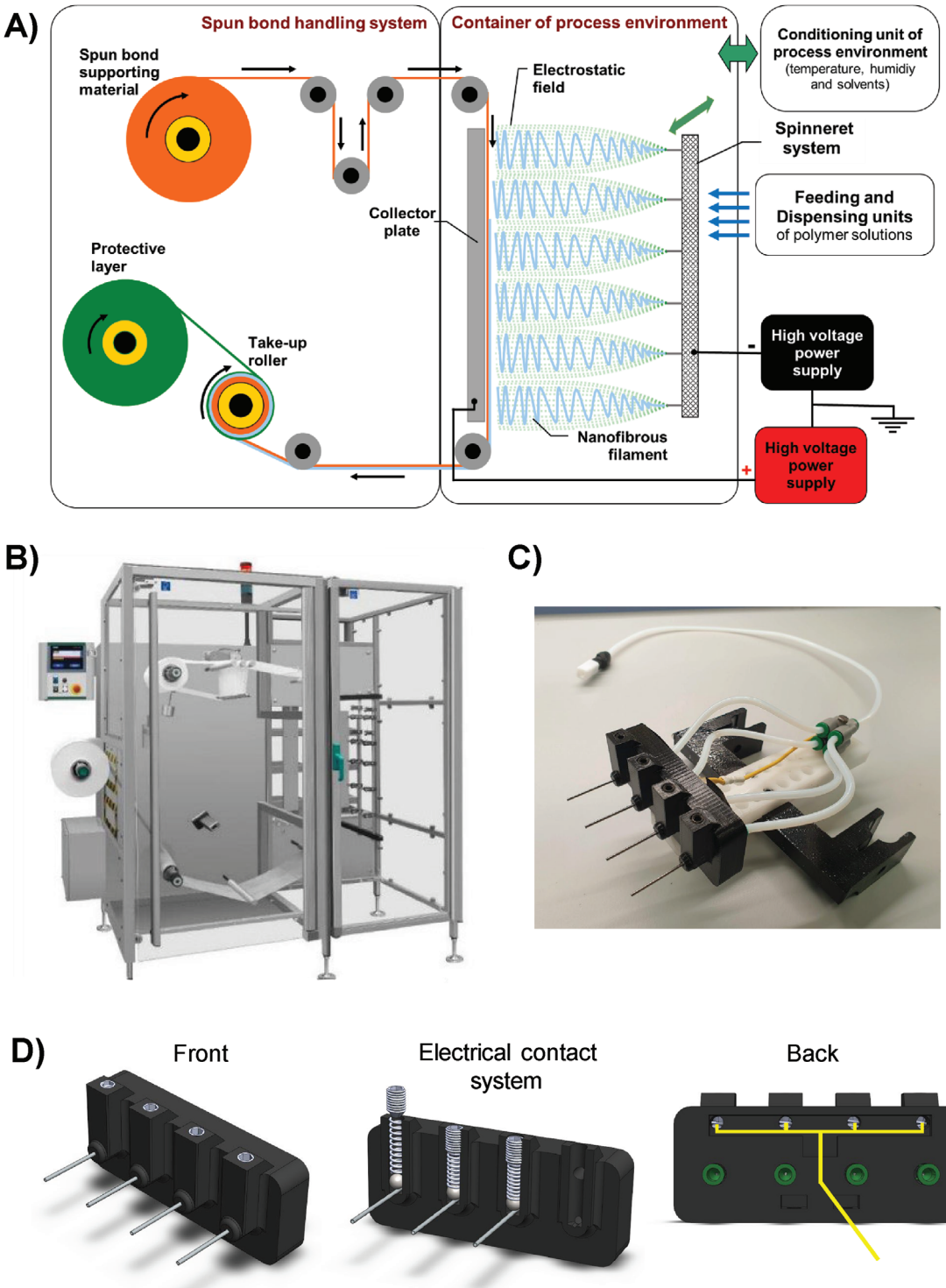

Figure 1. A) Multi-needle electrospinning setup for the production of filters. In the first chamber dedicated to the spunbond handling system, the pristine spunbond roll (orange line) is pulled by the take-up roller, maintaining constant tension through a system of dancer rollers and a constant speed via laser control. In the processing chamber, the spunbond passes in front of the counter electrode, getting coated with nanofibers (light blue line) from the spinneret system, which is positioned at an adjustable distance. The spinneret is fed by the dispensing unit of the polymer solution, consisting in six pumps. Both the spinneret and the counter electrode can be set at opposite and interchangeable potentials. The take-up roller collects the spunbond coated with nanofibers, also pulling another protecting layer of spunbond from another pristine spool (green line) in order to produce a 3-layered structure. B) Photograph of the machine; C) Example of a spinneret of the machine; D) schematic of the spinneret system: a blunt ended needle is inserted in each slot: to keep the electric contact with each needle, a spring (connected to a cable) is pre-tensioned by a set screw against a bearing ball which, in turn, press over the side of the metallic needle. The electric wires (yellow lines) connected to the springs are joined and connected to the high-voltage power supply.

then passes in front of a flat metal plate that acts as a counter-electrode inside the process chamber. The spinneret system, located at an adjustable distance in front of the counter-electrode, consists of a rack with six spinnerets. The rack can oscillate horizontally at an adjustable speed for a more uniform fiber deposition. The spinnerets (Figure 1C) are custom-designed. Each houses four commercially available blunt-ended needles (inner diameter = 0.84 mm) within a 3D-printed PET frame. In addition, the electrical contact system is concealed within the frame to avoid any solution leakage issues. Each needle chamber is equipped with a metal spring that is electrically connected to the high voltage by a cable and preloaded by a set screw (Figure 1D). The spring pushes on a metal ball which is housed in the needle socket. When the latter is inserted, the ball is pressed against the spring, ensuring electrical contact. Four PTFE tubes (inner diameter = 2 mm) feed the needles. The tubes are connected to a 4-way Y manifold, which is fed by a larger diameter tube. All needles in each spinneret operate at the same electrostatic potential. The spinnerets and the counter electrode plate are connected to two separate high voltage power supplies (SLM70N300 and SLM70P300, Spellman, Hauppauge, NY, USA), one negative, the other positive. A rack outside the machine, consisting of six different infusion pumps (NE-1000, New Era Pump Systems, Inc., Farmingdale, NY, USA), with 20 mL syringes, delivers the polymer solution to each spinneret. The entire machine is housed in a dedicated room where the temperature and relative humidity (RH) are maintained by a Mitsubishi air conditioner. The nanofiber-coated spunbond exiting the process chamber is collected by a motorized roller. During the collection phase, an additional layer of PP spunbond is deposited on the nanofiber side, resulting in a three-layer structure. A laser measures the accretion of the collection spool and adjusts the speed of the roller to maintain a constant sliding speed of the fabric in the process chamber. The collection spool can rotate to achieve a fabric sliding speed of up to 60 cm min^{-1}. Considering that approximately 17 cm of fabric is required to produce one face mask, the maximum productivity can be estimated at approximately 5000 face masks per day. All of the above automatic systems are controlled by a dedicated PLC with a touch screen interface. Prior to the fabrication of samples, the machine was extensively tested to verify its continuous production capability and materials quality. The process proved to be stable for several hours, with no clogging of the spinneret and no need for operator intervention. One aspect that still needs to be implemented to achieve true continuous production is the feed line. The laboratory-scale pumps currently in use contain syringes that can only store sufficient solution for a few hours, depending on the flow rate. The reloading phase is also the most delicate, as the probability of clogging is significantly higher during this period. To achieve continuous production, the feeding system by laboratory scale pumps can be replaced by an industrial commercially available continuous volumetric or peristaltic pump, which can feed directly from a reservoir, avoiding interrupting the process for refilling syringes.

2.3. Production and Characterization of Electrospun Filters

According to the results of the preliminary solution optimization presented in the Supporting Information (Table S1, Supporting Information), a 18% w V^{-1} PVDF solution in DMAc/AC 50/50 was selected.

The spinnerets were connected to a negative voltage (negative voltage electrospinning mode: NVES) and the counter electrode to a positive voltage. Incremental flow rates (from 4 to 8.5 mL h^{-1}, in steps of 0.5 mL h^{-1}, corresponding to a flow rate of 1 mL h^{-1} to 2.125 mL h^{-1} for each needle, Table S2, Supporting Information) were chosen to obtain electrospun filters with increasing values of nanofiber mass per unit area (grammage). The voltages applied to the counter electrode and the needles were adjusted for each flow rate to achieve a stable electrospinning process (Table S2, Supporting Information). The distance between the counter electrode and needles was set at 21 cm. The spunbond speed was 30 cm min^{-1} and the spinnerets rack swing was 5 cm s^{-1}. A total amount of 1.5 m of spunbond fabric covered with PVDF nanofibers was collected for each flow rate, corresponding to an electrospinning time of 5 min.

The grammage was calculated for each family of samples normalizing the total amount of polymer deposited on the spunbond during its passage across the counter-electrode to the surface area of the spunbond. For each flow rate, three 200 × 175 mm samples were cut from the three-layer structure; the ultrafine PVDF membranes were detached from the spunbonded PP layer, and their mass was measured using an analytical balance (AS 60/220, Radwag, Random, Poland).

To evaluate the effect of the spinneret polarity on the nanofiber surface potential, an intermediate flow rate was selected and, thanks to the flexibility of the setup, three other samples were produced with different modalities: (i) NVES with the counter electrode grounded, (ii) positive voltage electrospinning mode (PVES) with the counter electrode set to a negative voltage, and (iii) PVES with the counter electrode grounded (Table S3, Supporting Information). The distance between the counter electrode, the fabric speed, and the rack swing of the spinnerets were kept the same as above. The sample nomenclature includes a number for the flow rate employed and two letters indicating the polarity of the spinneret (first letter) and that of the counter-electrode (second letter) (P: positive, N: negative, G: grounded). For example, 50NP indicates a sample with a flow rate of 5.0 mL h^{-1}, applying a negative potential to the spinneret and a positive potential to the counter electrode.

The morphology of each sample was analyzed by scanning electron microscopy (SEM, Phenom Pro-X, Thermo Fisher Scientific, Waltham, MA, USA) on samples after gold sputtering. Fiber diameter was calculated as the average of 100 measurements using ImageJ software.

2.4. Investigation on Electrospinning Polarity

A non-contact electrostatic voltmeter (model TREK 341B, sensitivity +/−20 V) was used to determine the surface potential. The measurement is based on a field nulling technique for non-contact voltage measurement. The distance between the probe and the surface was set at 4 mm. For each material, 100 data were collected, and the mean and standard deviation of the surface potential were calculated.

2.5. Characterization of Assembled Face Masks

Face mask prototypes were tested according to the EN14683:2019 standard for surgical masks.[49] Pressure drop was measured on circular specimen of 25 mm in diameter using an airflow of 8 L min^{-1} after conditioning for at least 4 h at 85% RH at room temperature, as specified in the EN standard. The filtration performance of prototype masks was evaluated as BFE according to the EN standard. Circular samples of 80 mm in diameter were first conditioned at 85% RH at room temperature for at least 4 h and then placed in the BFE apparatus, where an airflow of 28.3 L min^{-1} was applied. A *Staphylococcus aureus* solution at a known concentration was nebulized onto the mask, using an atomizer, to obtain the droplet size distribution in compliance with the standard.

3. Results and Discussion

3.1. Morphological Characterization of Electrospun Filters

SEM examination of mats produced with NVES and counter-electrode connected to a positive voltage revealed randomly oriented homogeneous, smooth, and bead-free nanofibers (**Figure 2A**).

PVDF nanofibers were electrospun onto a layer of commercial spunbonded PP (fiber diameter 19.7 ± 1.77 µm), and an additional layer of spunbonded PP was placed on the electrospun mat for protective purposes. The resulting complete three-layer filter is shown in Figure 2B. For comparison, a micrograph of the internal structure of a commercially available surgical protective mask is shown in Figure 2G,H, in which the filtering layer is a nonwoven fabric made by the melt-blowing technique (a meltblown PP layer).[50] As can be seen by comparing Figure 2A,G, the meltblown fibers have a larger diameter (2.95 ± 2.04 µm) compared to the electrospun nanofibers.

The set of filters with increasing grammage obtained by increasing the flow rate exhibited a linear correlation between the grammage and the flow rate applied (Figure 2C and Table S4, Supporting Information). This finding is highly significant because it allows accurate prediction of nanofiber coverage on the filter based on the chosen flow rate. The linear correlation in the data validates the process efficiency, indicating minimal loss of nanofibers during electrospinning and their successful deposition on the collector. Figure 2D and Table S4 (Supporting Information) show the nanofiber diameters, represented by their mean value and standard deviation, as a function of the flow rate used to produce each sample. Despite the known dependence between these two parameters,[51] no trend is discernible, as confirmed by the morphological similarities of the nanofibers produced at minimum (Figure 2E) and maximum flow rates (Figure 2F).

The distribution of diameters has a high standard deviation, suggesting that a possible correlation trend between nanofiber diameter and flow rate may be hidden by the high experimental variability. This high standard deviation, associated with a broad fiber diameter distribution may be an advantage when considering the filtration performance of the membrane. Fibers of different diameters could improve the filtration due to the variety of pore dimensions, allowing for the separation of particles of different sizes.

The presence of fibers with different diameters in the same filter is exploited, for example, in air filters with a bimodal nanofiber diameter distribution in order to improve filtration by creating small pores with thin fibers, while microfibers contribute to improved airflow, breathability, and an increase in the effective filter area for particle retention.[52–54]

In addition, the presence of some fibers with larger diameters can increase the mechanical strength of the membrane, which is particularly useful in applications where the membrane may be subjected to high shear forces, as in the case of a protective mask, which is often subject to improper manipulation.

The polarity of the electrospinning appeared to affect the diameter of the nanofibers; using the same process parameters, NVES produced nanofibers with a smaller diameter (50NP = 0.39 ± 0.22 µm) than PVES (50PN = 0.53 ± 0.20 µm). The samples fabricated with the grounded counter electrode also showed the same behavior (50NG = 0.56 ± 0.29 µm vs 50PG = 0.63 ± 0.22 µm). Comparing the samples obtained with NVES (50NP and 50NG), the average diameter is smaller in the first case. Connecting the counter electrode to the opposite potential is known to be a good strategy to enhance the electric field between the spinneret and the counter electrode, leading to the formation of fibers with smaller diameters. Therefore, all other conditions being equal, the mat obtained by NVES and positively charged counter electrode provided the nanofibers with a smaller diameter, an advantageous feature for the construction of a filter that maximizes the bacterial and viral blocking performances.[18] Considering all of the above, the diameter of the nanofibers was calculated on the entire population of electrospun samples fabricated by NVES with counter electrode connected to a positive voltage, resulting in 0.41 ± 0.19 µm.

3.2. Surface Potential Analysis of Electrospun Filters

The residual electret surface potential (SP) generated by electrospinning is essential to improve filtration performance. Small respiratory droplets and particles sized between 0.2 and 0.5 µm are best filtered by electrostatic filtration, while other mechanical filtration methods, such as diffusion and interception, are less effective.[2] In the literature, the relationship between the polarity of the spinneret and the polarity of the surface potential is contradictory. Previous experiments on poly(D,L-lactic acid) (PDLLA) and poly(lactic-co-glycolic acid) (PLGA) have shown that PVES leads to the formation of a positive surface potential on the mats and NVES to a negative one.[40–42] However, in the case of PVES of PVDF, both positive surface potential[18,55] and negative surface potential[34,56] have been reported. In this work, the samples produced with both NVES and PVES showed a negative surface potential, but PVES resulted in a much smaller amplitude. The investigation of nanofiber mats (**Figure 3A** and Table S5, Supporting Information) showed that NVES yields about three times higher absolute surface potential values than PVES (SP_{50NP} = −339 ± 108 V and SP_{50PN} = −108 ± 186 V), as can be seen by comparing filters produced with an equal potential difference, but with the opposite polarity between the spinneret and counter electrode. This result is consistent with the findings of previous

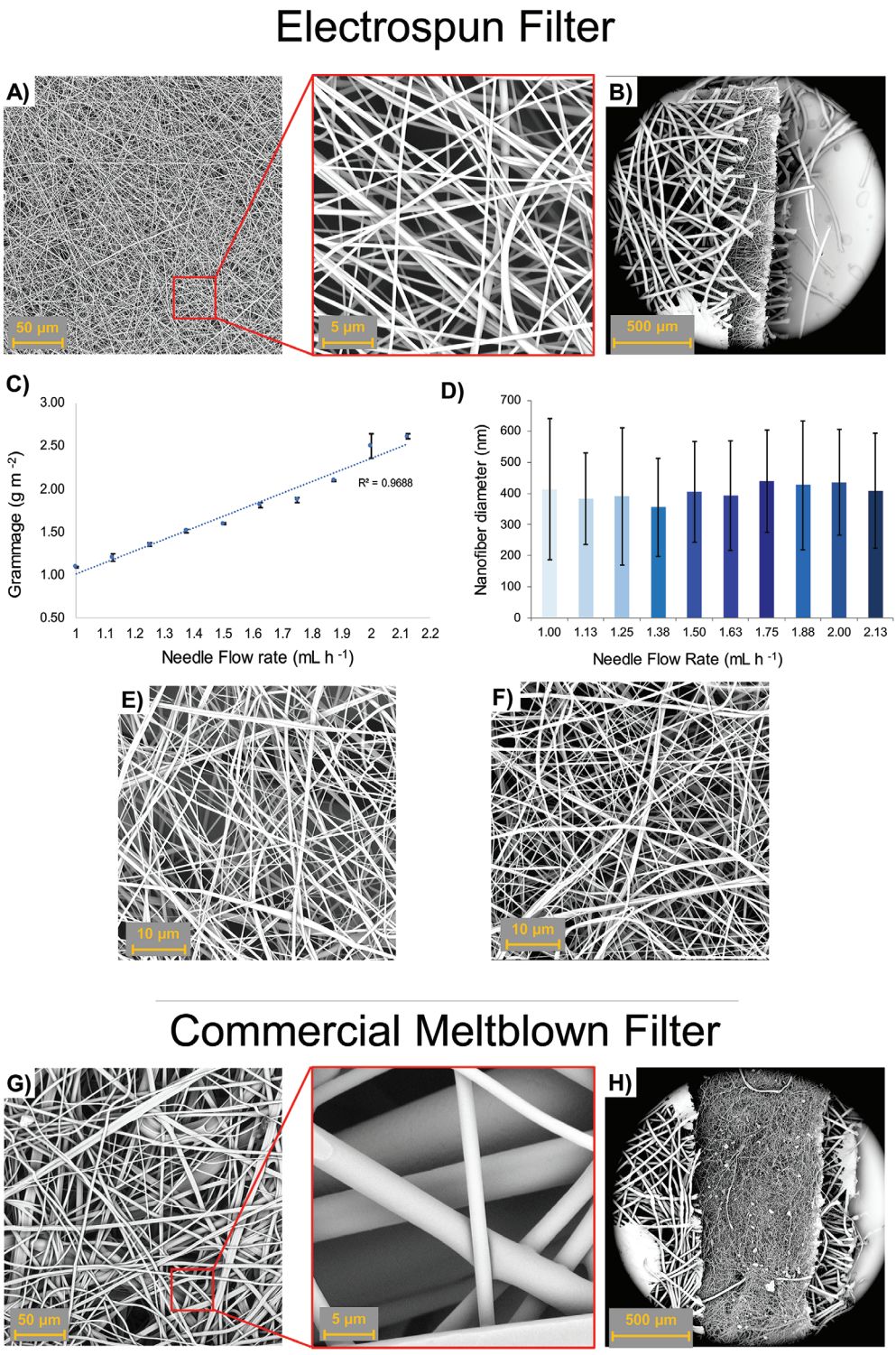

Figure 2. SEM micrographs of A) electrospun filter (60NP sample); B) three-layer filter composed of spunbond (left) -electrospun mat (center) – spunbond structure (right) (60NP sample). C) Electrospun mats grammage as a function of the single needle flow rate; D) fiber diameter distribution of samples produced with NVES as a function of the single needle flow rate; E) electrospun filter (40NP sample) produced with the lowest flowrate; F) electrospun filter (85NP sample) produced with the highest flow rate; G) SEM micrographs of a commercial meltblown filtering layer; H) three-layer filter spunbond (left)–meltblown (center) – comfort layer structure (right).

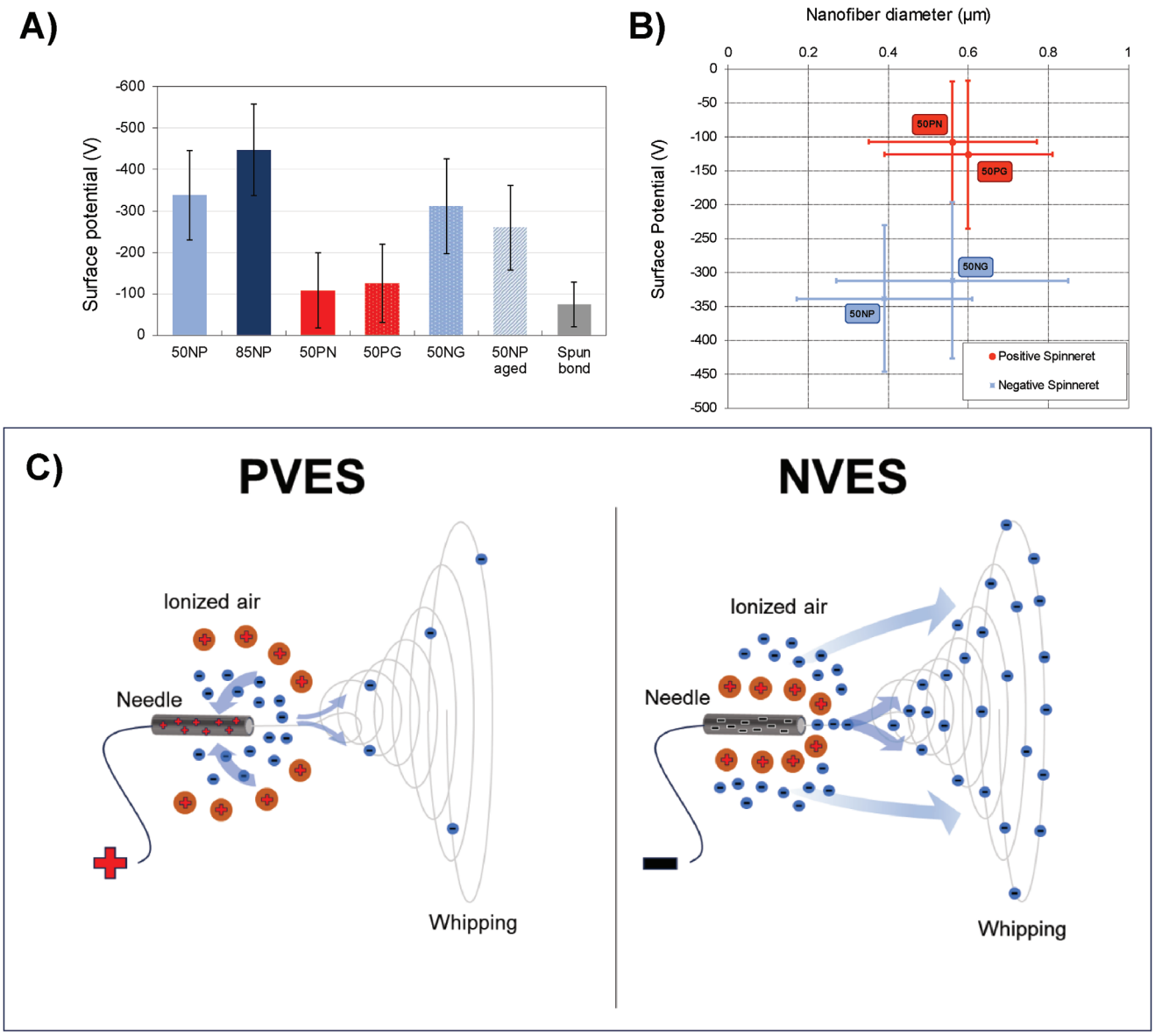

Figure 3. A) Surface potential measurements of electrospun mats produced with different combinations of polarities applied to the spinneret and the counter electrode; B) Investigation of the relationship between the surface potential and the nanofibers' mean diameter; C) proposed behavior of electrical charges in the two polarization modes of electrospinning process (electrons are represented by the blue points).

studies on electrospinning polarity, albeit carried out on different polymers.[39–42] The spunbond was also tested and showed a negative mean potential ($SP_{SPUNBOND} = -74 \pm 55$ V). The slightly negative surface potential of the latter is probably due to the accumulation of electrostatic charge from the friction of the spunbond on itself, which is supplied in the form of rolls of fabric.

To exclude that the surface potential of the mats was influenced by the voltage applied to the counter electrode, the mats produced with the grounded counter electrode were also tested. As shown in Figure 3A and Table S4 (Supporting Information), there is no substantial difference between the 50PN and the 50PG samples ($SP_{50PN} = -108 \pm 186$ V, $SP_{50PG} = -126 \pm 94$ V) and between the 50NP and 50NG samples ($SP_{50NP} = -339 \pm 108$ V, $SP_{50NG} = -312 \pm 115$ V). Furthermore, the surface potential of the mats does not seem to be related to the diameter of the nanofibers. As shown in Figure 3B, the critical discriminator in determining the surface potential value is the polarity of the spinneret. Thus, a possible explanation for the different amplitudes of the surface potential obtained with the two electrospinning modalities is sketched in Figure 3C: the electrospinning process involves ionization of the air in the proximity of the needle and the strong electronegativity of the fluorine atoms in PVDF efficiently traps negative charges.[24,55] In the case of PVES, the positively charged needle also attracts electrons, reducing the number of electrons available for the nanofiber. Conversely, in the case of NVES, the needle not only serves as an electron source, but also arranges the ionized charges to facilitate the interaction between the free electrons and the polymer jet of the newly formed

nanofiber. These electrons are then captured by the fluorine atoms.

With respect to the results obtained via NVES, increasing the grammage of the filter (increasing the process flow rate) also increases the surface potential (SP_{50NP} = −339 ± 108 V, SP_{85NP} = −447 ± 111 V). This can be attributed to both an increased amount of material under the probe and a tendency to enhance β-PVDF formation by increasing flow rates and potential during electrospinning.[57] The absolute values of surface potential obtained here with NVES are overall increased compared to previous work based on the PVES of PVDF electrets.[18,34,55,56] In addition, other research studies report laborious strategies to increase the surface potential, such as using the corona discharge technique,[48] triboelectrification,[32] or adding nanoparticles as charge enhancers.[18] On the contrary, in this work, the negative voltage electrospinning process itself enhances the surface potential, reducing the steps required to obtain highly charged filters, making them easier to manufacture, and increasing the productivity of the overall process.

It is also critical to consider the aging of these filters when comparing surface potential values, that is, the time elapsed since they were manufactured, as the induced charge is known to decay over time.[58,59] The surface potential data presented in this paper were collected 24 h after manufacture, a time when other studies have suggested that the transient with the most significant charge decay has ended.[58,59] Charge decay with time was also investigated. The surface potential of the 50NP sample was measured 12 months after production with a value of $SP_{50NPaged}$ = −260 ± 102 V, demonstrating good retention of surface potential despite some decay (sample one day after fabrication: SP_{50NP} = −339 ± 108 V).

3.3. Performance Analysis of Assembled Masks

Materials developed for medical devices must meet strict regulations. In the case of surgical face masks, the current standard in Europe is EN14683:2019,[38] which details all the tests required to certify a medical device. According to EN14683, all tests must be performed on the finished product or on pieces cut from the product. For this reason, thanks to the collaboration with KVM Engineering, wearable and fully assembled surgical mask prototypes were produced on a pneumatically operated automatic machine. Samples produced in the NVES mode with the counter electrode set to a positive potential were selected for their higher surface potential and smaller nanofiber diameter. As shown in the inset of **Figure** 4A, the masks were three-layered, with a central nanofiber layer surrounded by two layers of blue PP spunbond. Irritation and sensitivity tests were conducted by a third-party laboratory following a previously reported protocol,[60] to assess the safety of the materials according to the ISO10993:2018 standard (see Supporting Information). The prototypes were found to comply with current regulations for face mask materials.

It should be noted that materials produced at the laboratory scale and in academic laboratories are not commonly tested according to standards. This is primarily due to the challenges associated with producing samples of sufficient size and quantity as well as the high cost and limited availability of the necessary instrumentation and conditions required to perform such tests. Although several studies have been conducted on materials designed for facemask applications,[61,62] the characterization of the breathability and filtration efficiency of these filters has mostly been performed using homemade apparatus or without adherence to the standard. Therefore, the interpretation of the results could be difficult, and the comparison of proposed materials could be challenging.[63] The novel electrospun face mask materials produced in this work were tested according to the current standard.

The implementation of the pre-industrial multi-needle electrospinning setup enabled the fast and easy production of samples of sufficient area and uniformity to be characterized, with a production capacity of more than 5000 masks per day. Moreover, an application-oriented evaluation of the novel materials was carried out in order to have a complete set of information that can be easily used in the perspective of industrial production. The EN14683:2019 standard specifies the breathability requirements (upper limit: 40 Pa cm^{-2} for Type I and Type II masks, 60 Pa cm^{-2} for Type IIR masks) for face masks. As previously described, electrospun face mask materials are composed of three layers, with the middle layer being the actual electrospun filter layer. The external layers are made of spunbond PP, and their contribution to the respiratory resistance was found to be negligible (4.11 ± 0.40 Pa cm^{-2}) (see breathability values for the different samples in Figure 4B and Table S6, Supporting Information).

Since the main discriminator between samples is the flow rate imposed on the spinneret, it is reasonable to expect that samples produced at a higher-flow rate will be characterized by a thicker nanofibrous layer (and thus a higher grammage) and consequently a higher pressure drop and thus higher breathing resistance. This relationship is shown in Figure 4B, where it can be seen that grammage values below 2.10 g cm^{-2} correspond to breathability values that comply with the EN14683:2019 limit for Type I and II face masks. In addition, all other samples with higher grammages displayed breathability values within the limits specified for Type IIR masks. Type IIR masks are required to pass an additional test to evaluate their resistance to a synthetic blood splash. To pass the splash test, the outer PP spunbond layer of Type IIR face masks is usually modified with a hydrophobic coating. The support material available for this work was not surface treated to be splash resistant, that is, with a waterproof coating; therefore, Type IIR is not be considered further.

Regarding the BFE tests, the standard requires Type I surgical masks to have a filtration efficiency equal to, or greater than 95%, while Type II masks are required to provide a minimum filtration efficiency of 98%. The BFE of the prototype mask produced with the lowest flow rate, that is, with the lowest grammage, was already above the threshold specified by the standard, namely 96.5% (Figure 4C,D). Facemasks produced with this filter already provide strong protection and are extremely comfortable, showing a low resistance to air permeation during breathing (breathability = 23.1 ± 1.74 Pa cm^{-2}). By increasing the filter grammage above 1.35 g cm^{-2}, the filters showed a BFE above 98%, suitable for Type II masks. The sample with a grammage of 1.52 g cm^{-2} showed a BFE of 99.6%, while the sample with a grammage of 1.82 g cm^{-2}, showed a maximum filtration efficiency with a BFE of 99.9%. Considering the behavior of BFE as a function of grammage and the expectation of similar results for

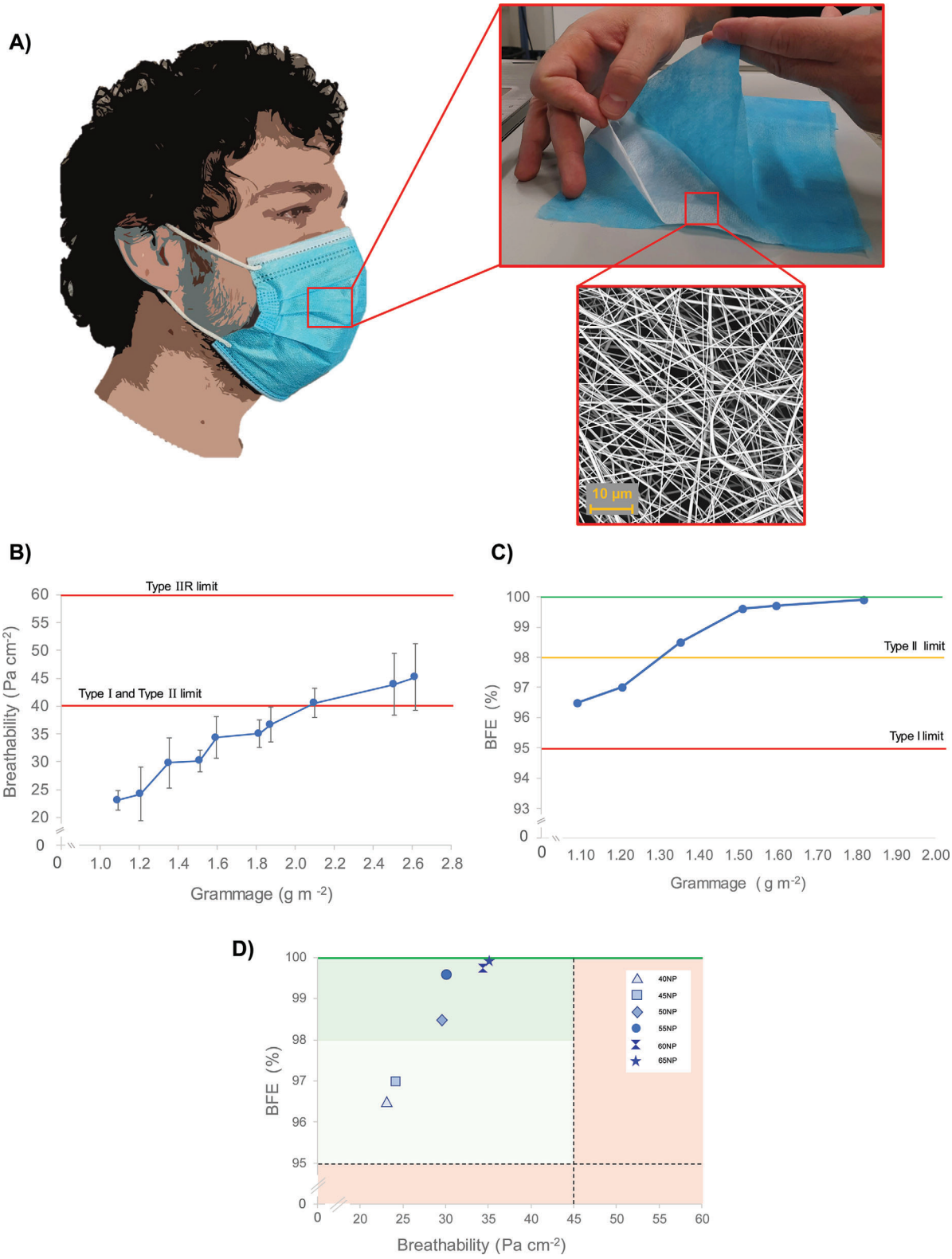

Figure 4. A) Assembled surgical mask with nanofibrous filtering layer. First inset: the three-layer structure, second inset: a detail of the nonwoven mat; B) breathability values of the different samples as a function of the mats grammage; C) BFE values of the different samples as a function of the mats grammage; D) BFE as a function of breathability: red areas do not meet regulatory standard, light green meets both breathability and BFE Type I masks standard requirements, dark green meets both breathability and BFE Type II masks standard requirement.

Table 1. Breathability of commercial[49] and electrospun nanofibers masks compared to the EN14683 standard.

Mask Type	BFE standard requirement [%]	Breathability standard requirement [Pa cm^{-2}]	Breathability commercial masks [Pa cm^{-2}]	Breathability electrospun masks (this work) [Pa cm^{-2}]
Type I mask	≥ 95	≤40	32.9 ± 4.3	23.1 ± 1.7
Type II mask	≥ 98	≤40	35.0 ± 4.1	29.8 ± 4.5

materials obtained with higher flow rates, BFE tests on higher grammage samples were deemed as unnecessary and were not performed.

Typically, surgical masks consist of several layers, with the filtering layer being a meltblown PP. Replacing this layer with different materials is challenging, especially considering the restrictive requirements of standard such as EN14683.

A previous study by Boi et al.[49] found that out of 435 surgical mask prototypes using different technologies for the filtering layer, only 8 met the criteria for Type I regulations and 20 for Type II regulations. Notably, all of the certified prototypes used meltblown PP as the filtering layer. The average breathability values for these prototypes are listed in **Table 1**. It is noteworthy that the breathability values obtained for electrospun masks in this study are significantly lower than those obtained for commercial masks (23.1 ± 1.7 vs 32.9 ± 4.3 Pa cm^{-2} for Type I, and 29.8 ± 4.5 vs 35.0 ± 4.1 Pa cm^{-2} for Type II). Thus, the electrospun facemasks not only proved to be a viable alternative to PP meltblown in terms of manufacturing process and materials used but also offered significant advantages in terms of breathability and wearer comfort while maintaining extremely high filtration standard (Figure 4D).

4. Conclusion

In this study, the successful design, construction, and implementation of a customized pre-industrial multi-needle setup allowed for the electrospinning of uniform nonwoven filters, charaterized by nanofibers with small diameters and high surface potential, essential attributes for effective filtration of fine particles. These membranes exhibited enhanced filtration and breathability capabilities, meeting the stringent requirement of the European standard for surgical masks (EN14683:2019). The use of the negative voltage electrospinning technique allowed the simultaneous production of nanofibers with a small diameter (0.41 ± 0.19 µm), optimizing mechanical filtration, and high surface potential values (up to −447 ± 111 V), maximizing filtration through the electrostatic mechanism. The bacterial filtration efficiencies obtained were extremely high (up to 99.9%), well above European standard. At the same time, the proposed masks demonstrated a significant improvement in breathability (up to 29.8 ± 4.5 Pa cm^{-2} for Type II standard masks) compared to the most recent measurements of surgical masks available on the market. The preservation of the nanofiber surface potential over time was confirmed by measurements taken one year after production, indicating excellent charge retention and the maintenance of increased filtration performance over time. The electrospun surgical masks proposed in this study represent a major advancement over commercial face masks made with meltblown PP, offering substantial improvements in breathability and end-user comfort while maintaining extremely high filtration standard. The materials used have been shown to be safe based on specific irritation and sensitivity tests. Substantial increases in throughput compared to laboratory-scale processes have enabled the production of samples in quantities and sizes suitable for testing according to standard regulations for a fairer and more direct comparison with the performance of commercial and promising new filters. With a production capacity of more than 5000 masks per day, which can be easily increased, it moves completely out of the laboratory environment and becomes a product already suitable for large-scale production, which is still unusual for the electrospinning technology, even after decades of intensive research.

Supporting Information

Supporting Information is available from the Wiley Online Library or from the author.

Acknowledgements

The authors would like to thank the Marchesini Group (Via Nazionale 100, 40065 Pianoro, Bologna, Italy), the GVS S.p.A. (Via Roma 50, 40069, Zola Predosa, Bologna, Italy), and Polonord Adeste SRL (Via Clodoveo Bonazzi 7, 40013, Castel Maggiore, Bologna, Italy) for the equipment and expertise provided. The authors would like to acknowledge Giorgia Pagnotta and Filippo Grolli for their help in the early stages of the project and KVM Engineering S.r.l. (Largo Cavallotti 5, 31029, Vittorio Veneto, Treviso), leaded by Ing. Andrea Carpenè, for the valuable help with the surgical mask assemblage. This research was funded by the Tech4Mask project, innovative technologies for producing face masks with enhanced anti-viral and bacterial properties – POR FESR Regione Emilia-Romagna.

Conflict of Interest

The authors declare no conflict of interest.

Author Contributions

C.G. and M.T. contributed equally to this work. C.G., M.T., R.O., G.T., A.S., C.B., D.F., M.L.F., and A.Z. conceptualized the study. C.G. and M.T. wrote the original draft. C.G., M.T., R.O., and G.T. produced and tested the samples. C.G., G.T., A.S., and A.Z. developed and tested the multi-needle electrospinning system. A.Z., C.B., D.F., M.L.F., and A.S. reviewed and edited the draft. C.B., D.F., M.L.F., and A.Z. administrated the work and were responsible for the funding acquisition. All authors listed have made a substantial, direct, and intellectual contribution to the work and approved it for publication.

Data Availability Statement

The data that support the findings of this study are available from the corresponding author upon reasonable request.

Keywords

electrospinning, face mask, filtration, nanomaterials, surface potential

Received: December 11, 2023
Revised: January 18, 2024
Published online:

[1] M. H. Chua, W. Cheng, S. S. Goh, J. Kong, B. Li, J. Y. C. Lim, L. Mao, S. Wang, K. Xue, L. Yang, E. Ye, K. Zhang, W. C. D. Cheong, B. H. Tan, Z. Li, B. H. Tan, X. J. Loh, *Research* **2020**, *2020*, 1.
[2] A. Tcharkhtchi, N. Abbasnezhad, M. Zarbini Seydani, N. Zirak, S. Farzaneh, M. Shirinbayan, *Bioact Mater* **2021**, *6*, 106.
[3] M. Guo, H. Liang, Z. Luo, Q. Chen, W. Wei, *Fibers Polym.* **2016**, *17*, 257.
[4] M. Kerner, K. Schmidt, S. Schumacher, V. Puderbach, C. Asbach, S. Antonyuk, *Sep. Purif. Technol.* **2020**, *239*, 116548.
[5] M. Nifuku, Y. Zhou, A. Kisiel, T. Kobayashi, H. Katoh, *J. Electrost.* **2001**, *51–52*, 200.
[6] Y. Gao, E. Tian, Y. Zhang, J. Mo, *Appl. Mater. Today* **2022**, *26*, 101369.
[7] H. Gao, W. He, Y.-B. Zhao, D. M. Opris, G. Xu, J. Wang, *J. Membr. Sci.* **2020**, *600*, 117879.
[8] K. Selvaranjan, S. Navaratnam, P. Rajeev, N. Ravintherakumaran, *Environ. Chall.* **2021**, *3*, 100039.
[9] A. Sanyal, S. Sinha-Ray, *Polymers* **2021**, *13*, 1864.
[10] O. J. Ayodeji, M. M. O. Khyum, R. T. Afolabi, E. Smith, R. Kendall, S. Ramkumar, *J Hazard Mater Adv* **2022**, *7*, 100128.
[11] N. O. Muniz, S. Gabut, M. Maton, P. Odou, M. Vialette, A. Pinon, C. Neut, N. Tabary, N. Blanchemain, B. Martel, *Nanomaterials* **2022**, *13*, 9.
[12] M. Mirković, D. B. Stojanović, D. Mijailović, N. Barać, Đ. Janaćković, P. S. Uskoković, *Mater. Chem. Phys.* **2022**, *285*, 126103.
[13] V. S. Naragund, P. K. Panda, *Int. J. Environ. Sci. Technol.* **2022**, *19*, 10233.
[14] W. Liang, Y. Xu, X. Li, X.-X. Wang, H.-D. Zhang, M. Yu, S. Ramakrishna, Y.-Z. Long, *Nanoscale Res. Lett.* **2019**, *14*, 361.
[15] S. Yan, Y. Yu, R. Ma, J. Fang, *Polym. Adv. Technol.* **2019**, *30*, 1635.
[16] F. Zabihi, J. Reissner, A. Friese, M. Schulze, C. Nie, P. Nickl, L. Lehmann, P. Siller, C. Melcher, T. Schneiders, T. Gries, U. Rösler, R. Haag, *Adv. Mater. Technol.* **2023**, *8*, 2300141.
[17] X. Li, Y. Gong, *J. Chem.* **2015**, *2015*, 1.
[18] S. Wang, X. Zhao, X. Yin, J. Yu, B. Ding, *ACS Appl. Mater. Interfaces* **2016**, *8*, 23985.
[19] D. H. Kang, N. K. Kim, H. W. Kang, *Polymers* **2021**, *13*, 3235.
[20] R. He, J. Li, M. Chen, S. Zhang, Y. Cheng, X. Ning, N. Wang, *J. Hazard. Mater.* **2022**, *428*, 128239.
[21] H. Shen, Z. Zhou, H. Wang, M. Zhang, M. Han, D. P. Durkin, D. Shuai, Y. Shen, *Environ. Sci. Technol. Lett.* **2021**, *8*, 545.
[22] C. Akduman, *J Ind Text* **2021**, *50*, 1239.
[23] W. W. F. Leung, Q. Sun, *Sep. Purif. Technol.* **2020**, *250*, 116886.
[24] I. A. Borojeni, G. Gajewski, R. A. Riahi, *Fibers* **2022**, *10*, 15.
[25] K. O'Dowd, K. M. Nair, P. Forouzandeh, S. Mathew, J. Grant, R. Moran, J. Bartlett, J. Bird, S. C. Pillai, *Materials* **2020**, *13*, 3363.
[26] A. Cimini, E. Imperi, A. Picano, M. Rossi, *Appl. Mater. Today* **2023**, *32*, 101833.
[27] A. Haider, S. Haider, I.-K. Kang, *Arab J Chem* **2018**, *11*, 1165.
[28] A. Zucchelli, D. Fabiani, C. Gualandi, M. L. Focarete, *J. Mater. Sci.* **2009**, *44*, 4969.
[29] L. De Sio, B. Ding, M. Focsan, K. Kogermann, P. Pascoal-Faria, F. Petronela, G. Mitchell, E. Zussman, F. Pierini, *Chemistry* **2021**, *27*, 6112.
[30] A. Zakrzewska, M. A. Haghighat Bayan, P. Nakielski, F. Petronella, L. De Sio, F. Pierini, *ACS Appl. Mater. Interfaces* **2022**, *14*, 46123.
[31] M. A. Haghighat Bayan, C. Rinoldi, D. Rybak, S. S. Zargarian, A. Zakrzewska, O. Cegielska, K. Põhako-Palu, S. Zhang, A. Stobnicka-Kupiec, R. L. Górny, P. Nakielski, K. Kogermann, L. De Sio, B. Ding, F. Pierini, *Biomater. Sci.* **2024**, https://doi.org/10.1039/D3BM01125A.
[32] J.-Y. Yin, C. Boaretti, A. Lorenzetti, A. Martucci, M. Roso, M. Modesti, *Nanomaterials* **2022**, *12*, 962.
[33] Y. Salkovskiy, *A. Fadeev, Sci. Rep.* **2022**, *12*, 20850.
[34] K. S. Han, S. Lee, M. Kim, P. Park, M. H. Lee, J. Nah, *Adv. Funct. Mater.* **2019**, *29*, 1903633.
[35] H. Zhang, L. Jia, P. Li, L. Yu, Y. Liu, W. Zhao, H. Wang, B. Li, A. C. S. Appl, *Polym. Mater.* **2022**, *4*, 2081.
[36] H. Kim, S. Lee, Y. R. Shin, Y.-N. Choi, J. Yoon, M. Ryu, J. W. Lee, H. Lee, A. C. S. Appl, *Polym. Mater.* **2022**, *4*, 338.
[37] R. Saikaew, V. Intasanta, *Sep. Purif. Technol.* **2021**, *275*, 119171.
[38] Medical Face Masks- Requirements and Test Methods, European Commitee for Standardization, BS EN14683:2019.
[39] D. P. Ura, U. Stachewicz, *Macromol. Mater. Eng.* **2022**, *307*, 2100843.
[40] Q. L. Zhao, Y. Zhou, M. Wang, *Mater. Sci. Forum* **2015**, *815*, 385.
[41] H.-W. Tong, M. Wang, *Nano Life* **2012**, *2*, 1250004.
[42] H.-W. Tong, M. Wang, W. W. Lu, *Nanomed* **2013**, *8*, 577.
[43] H.-W. Tong, M. Wang, *Biomed. Mater.* **2010**, *5*, 054110.
[44] P. K. Szewczyk, A. Gradys, S. K. Kim, L. Persano, M. Marzec, A. Kryshtal, T. Busolo, A. Toncelli, D. Pisignano, A. Bernasik, S. Kar-Narayan, P. Sajkiewicz, U. Stachewicz, *ACS Appl. Mater. Interfaces* **2020**, *12*, 13575.
[45] P. K. Szewczyk, S. Metwally, J. E. Karbowniczek, M. M. Marzec, E. Stodolak-Zych, A. Gruszczyński, A. Bernasik, U. Stachewicz, *ACS Biomater. Sci. Eng.* **2019**, *5*, 582.
[46] F. Calavalle, M. Zaccaria, G. Selleri, T. Cramer, D. Fabiani, B. Fraboni, *Macromol. Mater. Eng.* **2020**, *305*, 2000162.
[47] Z. Zhang, D. Ji, H. He, S. Ramakrishna, *Mater Sci Eng R Rep* **2021**, *143*, 100594.
[48] C. Akduman, E. P. Akçakoca Kumbasar, *IOP Conf Ser Mater Sci Eng* **2018**, *460*, 012013.
[49] C. Boi, F. Borsetti, T. M. Brugo, M. Cappelletti, M. G. D. Angelis, S. Fedi, S. D. Giacomo, G. Foli, A. Garelli, U. Genchi, D. Ghezzi, C. Gualandi, E. Lalli, M. Magnani, A. Maurizzi, F. Mazzi, N. Mehrabi, M. Minelli, R. Montalbano, L. Morelli, S. Nici, A. Paglianti, K. Papchenko, N. F. Parisi, R. Onesti, S. Rapino, M. Reggio, M. Roselli, E. Ruggeri, L. Sabatini, et al., *Sep. Purif. Technol.* **2022**, *294*, 121180.
[50] R. R. Bresee, W.-C. Ko, *Int. Nonwovens J.* **2003**, *os-12*, 1558925003os-12.
[51] N. H. A. Ngadiman, M. Y. Noordin, A. Idris, D. Kurniawan, *Adv Mater* **2013**, *845*, 985.
[52] M., Lin, J., Shen, B., Wang, Y., Chen, C., Zhang, H., Qi, *RSC Adv.* **2023**, *13*, 30680.
[53] A. Toptas, M. D. Calisir, M. Gungor, A. Kilic, *Polym. Eng. Sci.* **2023**, *985*, pen26593.
[54] Y. Mei, Z. Wang, X. Li, *J. Appl. Polym. Sci.* **2013**, *128*, 1089.
[55] Q. Sun, W. W.-F. Leung, *Sep. Purif. Technol.* **2019**, *212*, 854.
[56] Y. Hu, Y. Wang, S. Tian, A. Yu, L. Wan, J. Zhai, *Macromol. Mater. Eng.* **2021**, *306*, 2100128.
[57] S. Gee, B. Johnson, A. L. Smith, *J. Membr. Sci.* **2018**, *563*, 804.
[58] B. Tabti, A. Antoniu, M. Plopeanu, B. Yahiaoui, B. Bendahmane, L. Dascalescu, *J Phys Conf Ser* **2011**, *301*, 012044.
[59] M. C. Plopeanu, P. V. Notingher, L. M. Dumitran, B. Tabti, A. Antoniu, L. Dascalescu, *IEEE Trans. Dielectr. Electr. Insul.* **2011**, *18*, 1393.
[60] T. Petrachi, F. Ganzerli, A. Cuoghi, A. Ferrari, E. Resca, V. Bergamini, L. Accorsi, F. Burini, D. Pasini, G. F. Arnaud, M. Piccini, L. Aldrovandi, G. Mari, A. Tomasi, L. Rovati, M. Dominici, E. Veronesi, *Int J Environ Res Public Health* **2021**, *18*, 5387.
[61] V. S. Naragund, P. K. Panda, *Emergent Mater.* **2022**, *5*, 261.
[62] W. Essa, S. Yasin, I. Saeed, G. Ali, *Membranes* **2021**, *11*, 250.
[63] H. Shen, M. Han, Y. Shen, D. Shuai, *ACS Environ Au* **2022**, *2*, 290.

